Automated microaneurysm detection method based on double-ring filter in retinal fundus images

Atsushi Mizutani*[a], Chisako Muramatsu[a], Yuji Hatanaka[b],
Shinsuke Suemori[a], Takeshi Hara[a], Hiroshi Fujita[a]
[a]Department of Intelligent Image Information, Graduate School of Medicine,
Gifu University, 1-1 Yanagido, Gifu-shi, Gifu 501-1194, Japan;
[b]School of Engineering, The University of Shiga Prefecture,
2500 Hassaka-cho, Hikone-shi, Shiga 522-0057, Japan

ABSTRACT

The presence of microaneurysms in the eye is one of the early signs of diabetic retinopathy, which is one of the leading causes of vision loss. We have been investigating a computerized method for the detection of microaneurysms on retinal fundus images, which were obtained from the Retinopathy Online Challenge (ROC) database. The ROC provides 50 training cases, in which "gold standard" locations of microaneurysms are provided, and 50 test cases without the gold standard locations. In this study, the computerized scheme was developed by using the training cases. Although the results for the test cases are also included, this paper mainly discusses the results for the training cases because the "gold standard" for the test cases is not known. After image preprocessing, candidate regions for microaneurysms were detected using a double-ring filter. Any potential false positives located in the regions corresponding to blood vessels were removed by automatic extraction of blood vessels from the images. Twelve image features were determined, and the candidate lesions were classified into microaneurysms or false positives using the rule-based method and an artificial neural network. The true positive fraction of the proposed method was 0.45 at 27 false positives per image. Forty-two percent of microaneurysms in the 50 training cases were considered invisible by the consensus of two co-investigators. When the method was evaluated for visible microaneurysms, the sensitivity for detecting microaneurysms was 65% at 27 false positives per image. Our computerized detection scheme could be improved for helping ophthalmologists in the early diagnosis of diabetic retinopathy.

Keywords: Fundus images, Diabetic retinopathy, Microaneurysm, Computer-aided diagnosis

1. INTRODUCTION

In Japan, there are approximately 8.2 million patients with confirmed diabetes and approximately 18.7 million patients with suspected diabetes [1]. Approximately 3 million are thought to suffer from diabetic retinopathy (DR). This disease can be prevented from causing blindness if it is treated at an early stage. However, it has been reported [2] that approximately 3,000 people have lost their vision following the onset of DR. Retinal fundus images captured using a fundus camera are used for the diagnosis of DR. Ophthalmologists usually examine the presence of hemorrhages, microaneurysms, and exudates in order to diagnose DR. By using fluorescein angiograms, ophthalmologists can detect hemorrhages and microaneurysms. However, in the case of mass screening, using fluorescein as a contrast medium for diagnosing DR is not feasible. Therefore, only those patients who show the possibility of having DR are thoroughly examined in a hospital. It is desirable to detect hemorrhages and microaneurysms on retinal fundus images without using the contrast medium; however, detection of hemorrhages and microaneurysms is difficult because of their low contrast in noncontrast images. Therefore, a computer-aided diagnosis (CAD) system for the detection of these lesions can help ophthalmologists and physicians who review the mass screening exams in diagnosing DR.

Recently, many studies have been conducted on automated detection of DR [3–8]. Fleming *et al.* proposed a method for the detection of microaneurysms by using a watershed transform on fluorescein angiograms [3]. Serrano *et al.* proposed a method for detecting microaneurysms by the region growing technique in order to analyze fluorescein angiograms [4]. Other groups have investigated methods that use regular retinal fundus images captured without using the contrast

*mizutani@fjt.info.gifu-u.ac.jp; phone +81-58-230-6519; fax +81-58-230-6514; www.fjt.info.gifu-u.ac.jp

medium. Usher *et al.* reported a method for detecting hemorrhages, microaneurysms, and exudates by using adaptive intensity thresholding combined with an edge enhancement operation [5]. Niemeijer *et al.* proposed a method for the detection of red regions by pixel classification and feature analysis [6]. The sensitivity and specificity of their method were 100% and 87%, respectively. Nagayoshi *et al.* [7] reported a method that included normalization processes in addition to Usher's method [5]. Grisan *et al.* proposed a method for detecting the dark lesions on the basis of local thresholding and pixel density [8]. On the basis of a dataset of 60 annotated images, they reported a mean detection rate of 94% for lesions present in an image.

We have been attempting to develop a synthetic fundus CAD system [9–14]. We previously proposed methods for detecting abnormal blood vessels to help ophthalmologists in the diagnosis of hypertensive retinopathy [9, 10]. Moreover, we investigated methods for detecting retinal nerve fiber layer defects (NFLDs) [11] and for calculating the cup-to-disc ratio (C/D ratio) [12] that can be useful in the diagnosis of glaucoma. In addition, a technique for obtaining the depth value from the stereo image pair of a retinal fundus in the 3-D reconstruction of the optic nerve head [13] was developed. We also proposed a method for detecting hemorrhages and exudates in retinal fundus images without using contrast medium [14].

The aim of the present study is to develop methods for detecting microaneurysms in noncontrast images of the retinal fundus. A microaneurysm is one of the early signs of the onset of DR. It appears as a point lesion darker than the surrounding regions in retinal fundus images. Figure 1 shows a retinal fundus image with a microaneurysm.

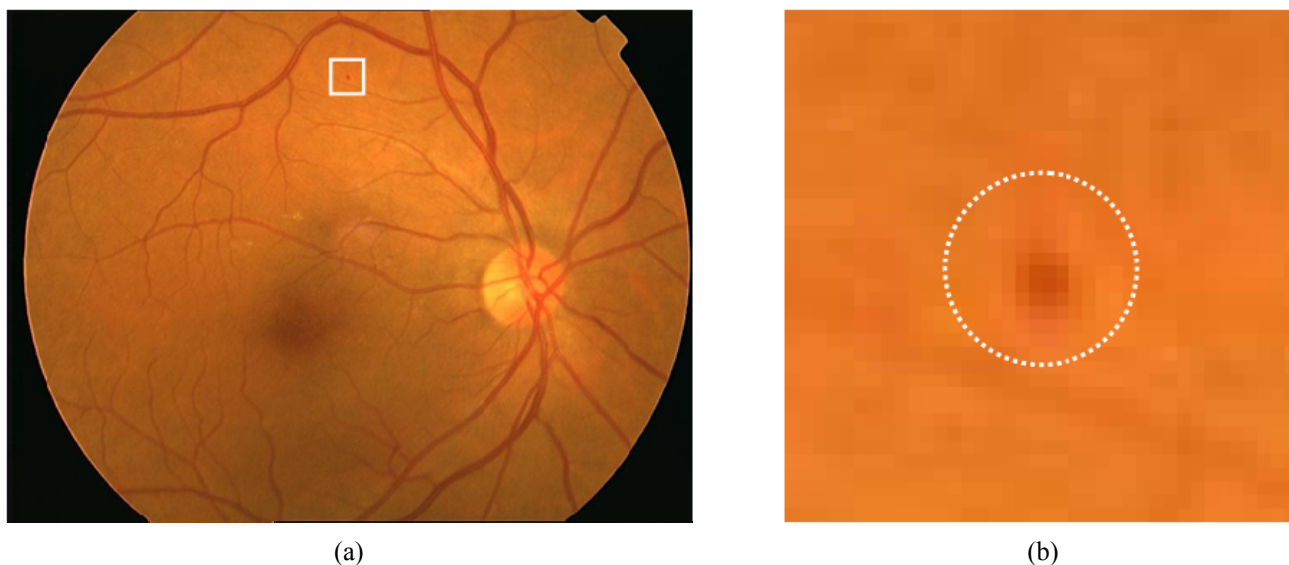(a)   (b)

Fig. 1. Example of a retinal fundus image with a microaneurysm. (a) Original retinal fundus image, and (b) enlarged image of the microaneurysm marked by a rectangle in (a).

2. MATERIALS AND METHOD

2.1 Database for this study

Retinal fundus images used in this study were distributed to interested researchers who desired to participate in the Retinopathy Online Challenge (ROC) [15] hosted by the University of Iowa. The database includes 50 retinal fundus images with "gold standard" locations of microaneurysms identified by a consensus of four ophthalmologists; these cases were intended to be used as a training set for the development of CAD systems. The ROC also includes 50 testing cases in which "gold standard" locations are not provided to the participants. For this reason, even though the results for the test cases are also included, training cases are mainly discussed in this paper.

The 50 training cases include RGB color images in three different image sizes: 768 × 576 pixels, 1059 × 1061 pixels, and 1389 × 1388 pixels; the number of images under each image size is 22, 3, and 25, respectively. Thirty-seven images include a total of 336 microaneurysms, whereas no microaneurysms were identified in the remaining 13 images. The number of microaneurysms identified in each of the 37 images ranges from 1 to 41.

2.2 Overall scheme for detection of microaneurysms

The flowchart of the overall detection scheme is shown in Fig. 2. First, images were preprocessed to reduce noise and variation in the brightness of the images. For simplicity in further processing of the images, the matrix sizes of the images were standardized to the largest one of the three different image sizes included in the database. The initial detection of the microaneurysms was attempted by applying the double-ring filter on the green channel of the color images; this was followed by the elimination of lesions in the blood vessels, which were false positives. Next, the shapes of the candidate lesions for an accurate determination of their image features were examined. Finally, the candidate lesions were classified as microaneurysms or false positives by the rule-based method and by using an artificial neural network (ANN).

```
          ┌─────────────────────────────┐
          │     Retinal fundus image    │
          └─────────────┬───────────────┘
                        ↓
          ┌─────────────────────────────┐
          │     Image preprocessing      │──────────┐
          └─────────────┬───────────────┘          │
                        ↓                           ↓
┌─────────────────────────────┐    ┌─────────────────────────────┐
│ Initial detection of        │    │  Extraction of blood vessels │
│ microaneurysms              │    └─────────────┬───────────────┘
└─────────────┬───────────────┘                  │
              ↓                                   │
┌─────────────────────────────┐                  │
│   Removal of blood vessels   │←─────────────────┘
└─────────────┬───────────────┘
              ↓
┌─────────────────────────────┐
│ Re-examination of candidate  │
│ lesions                      │
└─────────────┬───────────────┘
              ↓
┌─────────────────────────────┐
│ Determination of candidate   │
│ lesion features              │
└─────────────┬───────────────┘
              ↓
┌─────────────────────────────┐
│  Reduction of false positives│
└─────────────────────────────┘
```
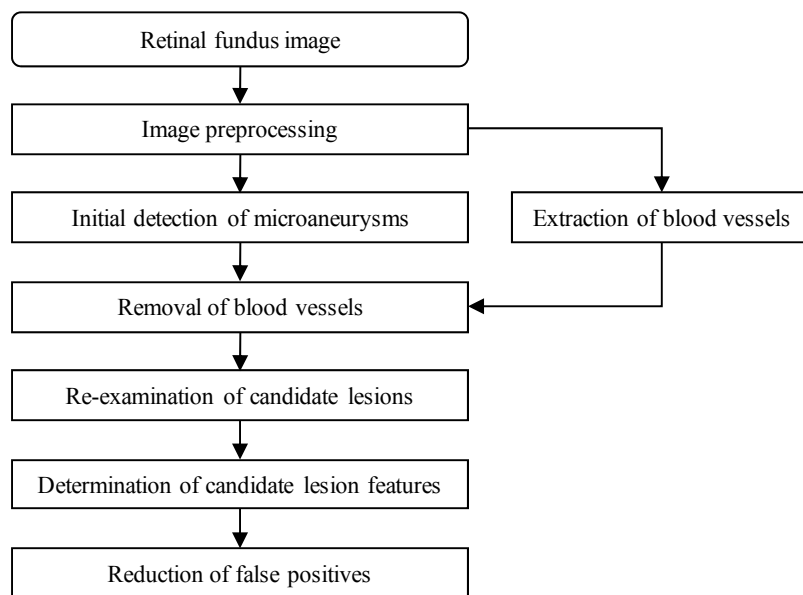
Fig. 2. Flowchart of overall scheme for detection of microaneurysms. The extraction of blood vessels from the images is incorporated for removing the false positives in the detected regions of the blood vessels.

2.3 Image preprocessing

The differences in brightness and colors of the retinal fundus images were due to the photographic conditions. In order to reduce these differences, brightness correction, gamma correction, and contrast enhancement [14] were applied to each image. The contrast of microaneurysms tends to be high in green color; therefore, RGB color images were converted to green-channeled images. Because the ROC database includes images with three different sizes, smaller images were enlarged using a bicubic convolution method so that their widths were unified to those of the largest images. The aspect ratio of each image was the same as that of the original image. Because the image noise may also be amplified, a median filter of dimensions 3 × 3 pixels was applied for reducing the image noise.

2.4 Initial detection of microaneurysms

Microaneurysms appear as lesions darker than the surrounding retinal regions. Therefore, it was expected that microaneurysms could be detected by using a double-ring filter [10], which compares the target pixel values with the neighboring pixel values. The filter consists of an inner circle and an outer ring with diameters of 5 and 13 pixels,

respectively. If the average pixel value in the inner circle was lower than the surrounding pixels in the outer ring region for a certain amount, the pixel in question became a candidate pixel for microaneurysms. In this study, the maximum number of candidate lesions for microaneurysms in each image was limited to 300.

2.5 Removal of blood vessels appearing as false positives

After the initial detection of microaneurysms, many blood vessels appeared as false positives in the preprocessed green-channeled images. In order to eliminate these false positives, the pixels corresponding to the part of the blood vessels were extracted by using the double-ring filter. This double-ring filter had an inner circle and outer ring with diameters of 7 and 21 pixels, respectively.

The initially detected candidates were superimposed onto the images of the extracted blood vessels. Lesions that were detected in the blood vessel regions were considered as false positives and removed from the candidates.

2.6 Re-examination of candidate lesions

The shapes of candidate lesions after the initial detection are affected by the structure of the double-ring filter. Therefore, the shapes of candidate lesions were not determined accurately, which could influence the accuracy of image feature analysis. In order to determine the shapes of candidate lesions correctly, their shapes were re-examined. On the basis of the remaining candidate pixels after the removal of false positives, neighboring pixels with comparable pixel values were included in the candidate lesions.

2.7 Feature determination and reduction of false positives

The candidate lesions in the initial detection process included numerous false positives. Therefore, in order to remove the false positives, 12 image features were calculated for each candidate lesion. The 12 features included (1) area, (2) degree of circularity, (3) length-to-width ratio [16], (4–6) mean value of the candidate lesion in each of the red, green, and blue bits, (7–9) difference between the maximum and minimum pixel values of the candidate lesion in each of the red, green, and blue bits, and (10–12) contrast, which is defined as the difference between the mean value of the candidate lesion and the mean value of the surrounding regions in each of the red, green, and blue bits.

The surrounding regions mentioned in features (10–12) are defined as the pixels that are separated by less than two pixels from the border of the candidate lesion; the pixels are determined by dilation operation. Figure 3 shows the regions of a candidate lesion marked as "A" and its surrounding regions marked as "B."

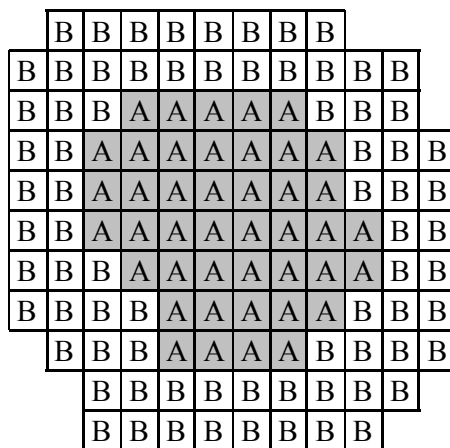|		B	B	B	B	B	B	B			
	B	B	B	B	B	B	B	B	B	B	
	B	B	B	A	A	A	A	B	B	B	
	B	B	A	A	A	A	A	A	B	B	B
	B	B	A	A	A	A	A	A	B	B	B
	B	B	A	A	A	A	A	A	A	B	B
	B	B	B	A	A	A	A	A	A	B	B
	B	B	B	B	A	A	A	A	B	B	B
		B	B	B	A	A	A	B	B	B	B
			B	B	B	B	B	B	B	B	
			B	B	B	B	B	B	B		

Fig. 3. Example of candidate lesion marked as "A" and surrounding regions marked as "B," which are used for determining the contrast.

On the basis of these features, candidate lesions were classified as microaneurysms or false positives using the rule-based method and an ANN. For the ANN, a three-layered feed-forward network with a back-propagation algorithm was employed. The number of input features was varied from 1 to 12. The classification utility of each feature was determined by discriminant analysis. The number of features was decreased one by one from 12 to 1 by removing the features with the lowest utilities. The number of hidden units was also varied along with the number of input units. For avoiding over-training of the ANN, the training was stopped at a certain iteration number.

2.8 Evaluation of computerized detection method

The results of our CAD system were evaluated by use of the free-response receiver operating characteristic (FROC) analysis. If the barycenter of a candidate lesion was within a certain distance from the "gold standard" location of the microaneurysms, the result was considered as a true positive detection.

The ROC cases include many microaneurysms that are very difficult to detect. Therefore, the visibilities of the microaneurysms used in this study were evaluated individually by the two co-authors (A.M. and C.M.). They were unblinded to the "gold standard" locations. As a result, 140 out of 336 microaneurysms, 42 percent of all, were determined invisible by both co-authors. Figure 4 shows the green-channeled image of a visible microaneurysm and the green-channeled image of an invisible microaneurysm. The contrasts of invisible microaneurysms in relation to the surrounding retinal regions are considerably lower than those of visible microaneurysms to the surrounding retinal regions.

It appeared that the detection of these invisible microaneurysms was extremely difficult, if not impossible. Even if these microaneurysms were detected by the CAD system, ophthalmologists reviewing the computer outputs would probably ignore them. Therefore, for the training cases, the results of our computerized scheme were evaluated in two ways: the sensitivities were determined for all microaneurysms and for visible microaneurysms only.
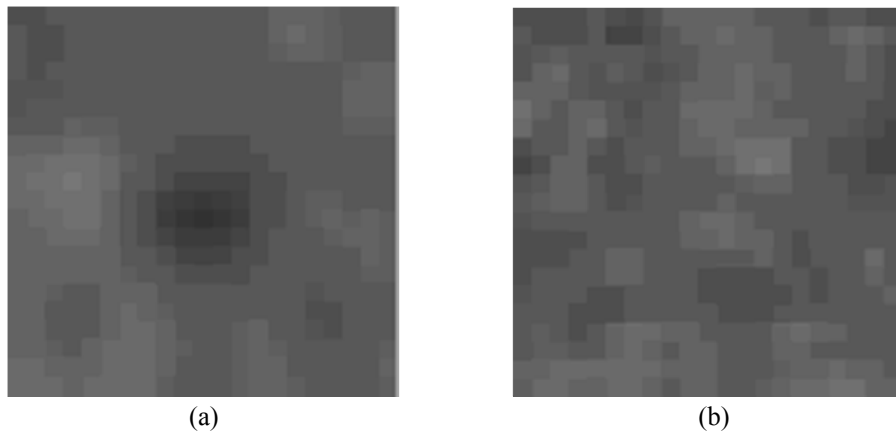

(a) (b)

Fig. 4. (a) Green-channel image of a visible microaneurysm and (b) green-channeled image of an invisible microaneurysm. The "gold standard" locations of microaneurysms are at the center of these images.

3. RESULTS

The true positive fractions (TPFs) and the number of false positives per image (FPI) after the initial detection, the classification by the rule-based method, and the classification by the ANN for the training cases are summarized in Table 1. The TPFs for the 196 visible microaneurysms are also shown in Table 1. The results indicate that detection of microaneurysms in the images of the ROC database is very difficult.

The computerized scheme was applied for the 50 test cases, and the test results obtained using the trained ANN were submitted to the ROC organizers. Figure 5 shows FROC curves obtained for all microaneurysms and only visible microaneurysms in the training cases and for the test cases. It is apparent in Fig. 5 that the sensitivity for detecting visible microaneurysms was considerably higher than that for "invisible" microaneurysms. The performance for the 50 test cases was comparable to that for the visible microaneurysms in the training cases. Because the "gold standard" locations of microaneurysms in the test cases were not provided, detailed analysis of the results for the test cases was not possible. The results could be due to the difference in difficulty levels for detecting microaneurysms in the training and test datasets.

Table 1. True positive fractions (TPFs) and the numbers of false positives per image (FPI) after the initial detection process, false positive reduction using the rule-based method and ANN for the 50 training cases.

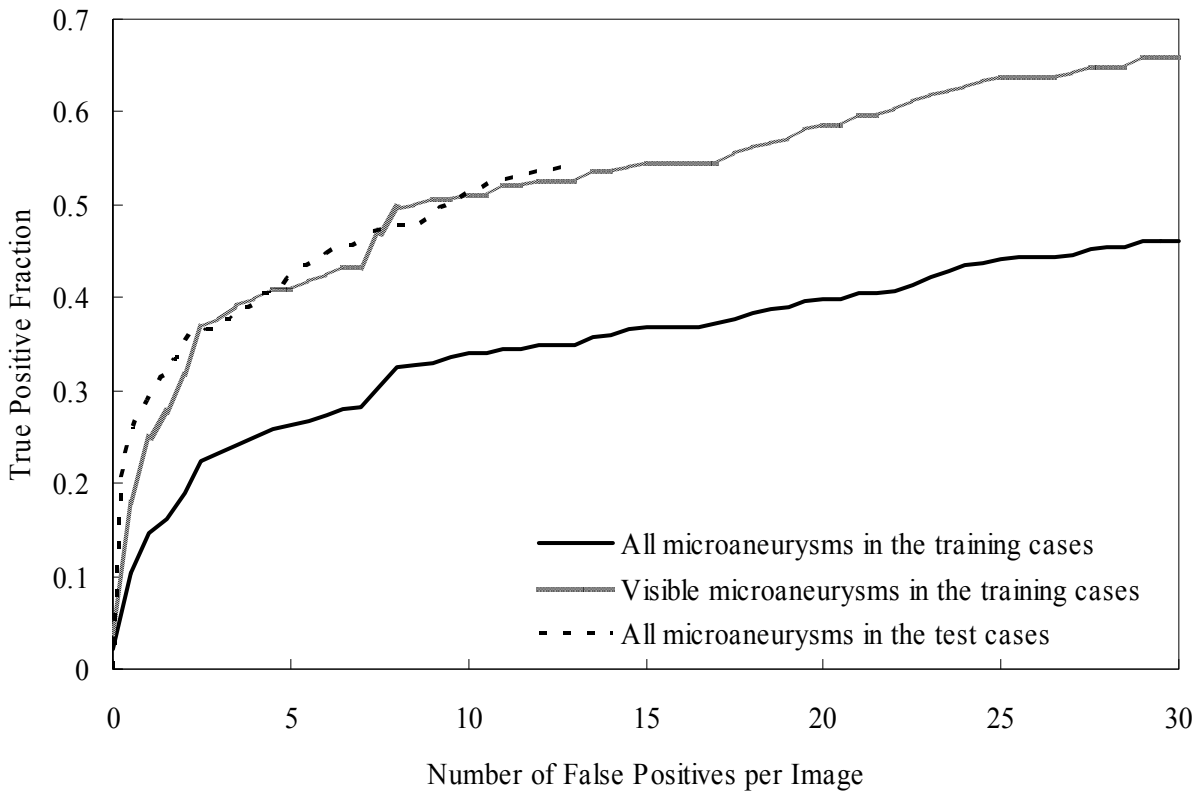|	TPF of all microaneurysms	TPF of visible microaneurysms	FPI
Initial detection	0.518 (174 / 336)	0.699 (137 / 196)	183.38 (9169 / 50)
Classification using the rule-based method	0.506 (170 / 336)	0.699 (137 / 196)	105.28 (5264 / 50)
Classification using an ANN	0.449 (151 / 336)	0.648 (127 / 196)	27.04 (1352 / 50)

Fig. 5. FROC curves for all microaneurysms and only visible microaneurysms in 50 training cases and that for 50 test cases.

4. DISCUSSION

False positives detected in the images can be grouped into two major categories: (1) capillary blood vessel regions that were not identified as the regions corresponding to the blood vessels and (2) noise regions. Figure 6 shows the green-channeled images of such false positives and the binary image of the lesions that were detected by the CAD system.

Because the accuracy of the extraction of blood vessels from the images was insufficient, reduction of some false positives in the blood vessel regions failed. The accuracy of extraction of large blood vessels from the images was relatively high, whereas it was low for the capillary blood vessels. In order to remove the false positives in the blood vessels, it is important to improve the accuracy of extraction of blood vessels from the images.

Further, one of the reasons for detecting noise as the candidates of microaneurysms was that noise reduction during preprocessing was not optimal. Moreover, block noise was prominent in some images. For these reasons, a selective noise reduction process that retains the contrast of microaneurysms is required.
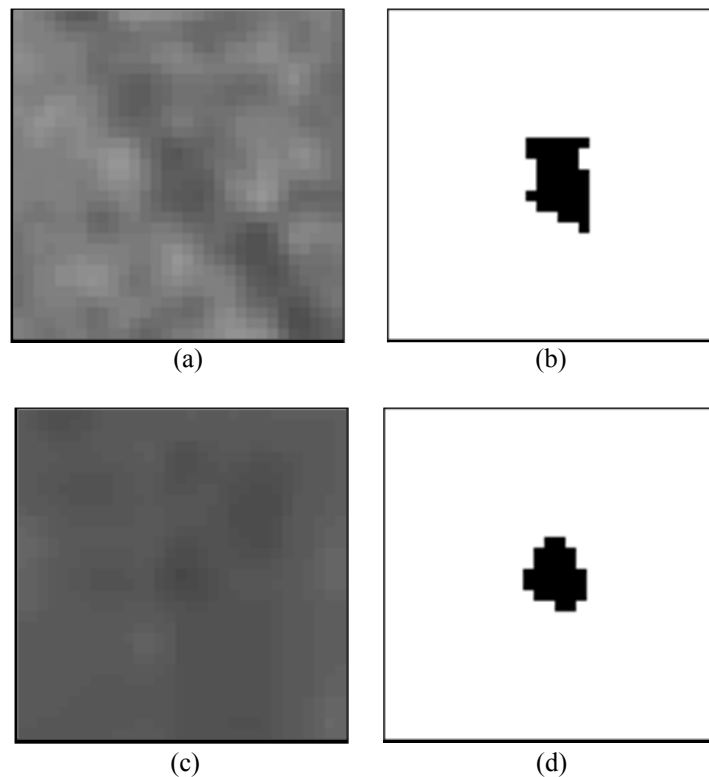

Fig. 6. Examples of false positives. (a) green-channeled image of a capillary blood vessel region, (b) detected regions of (a), (c) green-channeled image of noise regions, and (d) detected regions of (c).

5. CONCLUSION

We investigated a method for the automated detection of microaneurysms on retinal fundus images. We applied our method on the 50 training cases obtained from the ROC database; the sensitivity of our method was 45% when the number of false positives was 27 per image. Although this database includes extremely difficult cases, our method could be improved further for the detection of visible microaneurysms in order to facilitate the early diagnosis of DR.

ACKNOWLEDGMENTS

REFERENCES

[1] Ministry of Health, Labour and Welfare in Japan, [Overview of Japanese health and nutrition survey results in 2006], URL: http://www.mhlw.go.jp/houdou/2008/04/dl/h0430-2c.pdf (only available in Japanese), 29-30 (2008).

[2] S. Kinano, "Status of visual impairment in Japan," DIABETES NEWS, Diabetes Center at Tokyo Women's Medical University homepage, URL:http://www.dm-net.co.jp/twmu/news/094.htm (only available in Japanese).

[3] A. D. Fleming, S. Philip, K. A. Goatman, J. A. Olson, and P. F. Sharp, "Automated microaneurysm detection using local contrast normalization and local vessel detection," IEEE Trans. Medical Imaging 25, no. 9, 1223–1232 (2006).

[4] C. Serrano, B. Acha, and S. Revuelto, "2D adaptive filtering and region growing algorithm for the detection of microaneurysms", in Proc. SPIE Medical Imaging 2007: Image Processing 5370, 1924–1931 (2004).

[5] D. Usher, M. Dumskyj, M. Himaga, T. H. Williamson, S. Nussey, and J. F. Boyce, "Automated detection of diabetic retinopathy in digital retinal images: a tool for diabetic retinopathy screening", Diabetic UK Diabetic Medicine, 21, no. 1, 84–90 (2004).

[6] M. Niemeijer, B. V. Ginneken, J. Staal, M. S. Suttorp-Schulten, and M. D. Abramoff, "Automatic detection of red lesions in digital color fundus photographs", IEEE Trans. Medical Imaging, 24, no. 5, 584–592 (2005).

[7] H. Nagayoshi, Y. Hiramatsu, T. Kagehiro, Y. Mizuno, M. Himaga, H. Sakou, S. Sato, H. Fukushima, and S. Kato, "Detection of lesions from fundus images for diagnosis of diabetic retinopathy", IEICE Technical Report, 105, no. 64, 61–66 (2005).

[8] E. Grisan, A. Ruggeri, "Segmentation of candidate dark lesions in fundus images," in Proc.29th IEEE EMBS, Lyon, France, 6735-6738 (2007).

[9] Y. Hatanaka, T. Nakagawa, Y. Hayashi, A. Aoyama, X. Zhou, T. Hara, H. Fujita, Y. Mizukusa, A. Fujita, and M. Kakogawa, "Automated detection algorithm for arteriolar narrowing on fundus images," in Proc. 27th IEEE EMBS, Shanghai, paper#291 (2005).

[10] R. Takahashi, Y. Hatanaka, T. Nakagawa, Y. Hayashi, A. Aoyama, Y. Mizukusa, A. Fujita, M. Kakogawa, T. Hara, and H. Fujita, "Automated analysis of blood vessel intersections in retinal images for diagnosis of hypertension," Medical Imaging Technology 24, no. 4, 270–276 (2006).

[11] Y. Hayashi, T. Nakagawa, Y. Hatanaka, A. Aoyama, Y. Mizukusa, A. Fujita, M. Kakogawa, T. Hara, H. Fujita, and T. Yamamoto, "Detection of retinal nerve fiber layer defects in retinal fundus images using Gabor filtering," in Proc. SPIE Medical Imaging 2007: Computer-aided Diagnosis, San Diego, 6514, 65142Z-1-65142Z-8.

[12] Y. Hatanaka, Y. Hayashi, T. Nakagawa, A. Aoyama, X. Zhou, T. Hara, H. Fujita, Y. Mizukusa, A. Fujita, and M. Kakogoawa, "Development of Computer-aided Diagnosis System for Fundus Images," in 8th International Conference on Medical Image Computing and Computer-assisted Intervention: Short Paper, Palm Springs, CA, 2005, http://www.miccai2005.org.

[13] T. Nakagawa, Y. Hayashi, Y. Hatanaka, A. Aoyama, T. Hara, A. Fujita, M. Kakogawa, H. Fujita, and T. Yamamoto, "Three-dimensional reconstruction of optic nerve head from stereo fundus images and its quantitative estimation," in Proc. 29th IEEE Engineering in Medicine and Biology Conference Management System Annual International Conference, Lyon, 6747–6750 (2007).

[14] Y. Hatanaka, T. Nakagawa, Y. Hayashi, M. Kakogawa, A. Sawada, K. Kawase, T. Hara, and H. Fujita, "Improvement of Automatic Hemorrhages Detection Methods using Brightness Correction on Fundus Images," in Proc. SPIE Medical Imaging 2008: Computer-aided Diagnosis, 6915, 69153E-1-69153E-10(2008).

[15] The University of Iowa, the ROC organizers (Michael D. Abramoff, Bram van Ginneken and Meindert Niemeijer), "The ROC website," URL: http://roc.healthcare.uiowa.edu/index.php

[16] S. Kasai, H. Fujita, T. Hara, Y. Hatanaka, and T. Endo, "Elimination of funicular-shaped false-positive candidates in an automated detection algorithm for mammographic masses," in Journal of Computer Aided Diagnosis of Medical Images, 3, (1999).